Journal of Applied Polymer Science

Using Synchrotron FTIR Spectroscopy to Determine Secondary Structure Changes and Distribution in Thermoplastic Protein

James Michael Bier, Casparus Johannes Reinhard Verbeek, Mark Christopher Lay
School of Engineering, Faculty of Science and Engineering, University of Waikato, Hamilton 3240, New Zealand
Correspondence to: J. M. Bier (E-mail: jmb101@waikato.ac.nz)

ABSTRACT: Blood meal is a high protein, low value by-product of the meat processing industry that can be converted into a thermoplastic material by extrusion with a combination of a surfactant, urea, a reducing agent, water, and plasticiser. Changes in protein structure after each processing step (mixing with additives, extrusion, injection molding, and conditioning) were explored using synchrotron FTIR microspectroscopy. Blood meal particles were found to have higher β-sheet content around the perimeter with a randomly structured core. α-Helices were either located near the core or were evenly distributed throughout the particle. Structural rearrangement consistent with consolidation into a thermoplastic was seen after extrusion with processing additives, resulting in reduced α-helices and increased β-sheets. Including triethylene glycol as a plasticiser reduced α-helices and β-sheets in all processing steps. At all processing stages, regions with increased β-sheets could be identified suggesting blood meal-based thermoplastics should be considered as a semicrystalline polymer where clusters of crystalline regions are distributed throughout the disordered material.
 J. Appl. Polym. Sci. 130: 359–369, 2013

KEYWORDS: proteins; thermoplastics; spectroscopy; extrusion; microscopy

Received 9 December 2012; accepted 6 February 2013; published online 16 March 2013
DOI: 10.1002/app.39134

INTRODUCTION

Renewable alternatives to petrochemical polymers can be produced by converting biomass sources into new polymers (e.g., PLA or PHA) or by modifying biopolymers to enable thermoplastic processing. Thermoplastic starch is available commercially and thermoplastics have been produced from many proteins, including wheat, soy, and sunflower from plants as well as gelatine, keratein, casein, whey, and blood meal from animals.[1] Blood meal is a denatured protein by-product of the meat processing industry produced by steam coagulation and drying of blood. Treating blood meal with a combination of water, a protein denaturant, a reducing agent and a surfactant produces a thermoplastic, which can be extruded and injection molded.[2,3]

Proteins in their native and denatured states typically contain regions of secondary structures such as α-helices, β-sheets, and random coils. Extrusion and injection molding of proteins require chain rearrangement, implying changes to protein secondary structure. This structural rearrangement is a major challenge in developing protein-based thermoplastics.[4] For processing, existing chain interactions in and between proteins must be overcome using denaturants, reducing agents, surfactants, and heating, forming a homogenous melt, followed by new interactions forming during cooling to consolidate the molded or extruded article.[1,5] Although not exclusively the case, thermoplastic processing tends to increase β-sheet content at the expense of α-helices.[1] β-Sheets have stronger hydrogen bonding interactions than α-helices, potentially creating stronger interchain interactions and hence stronger materials. For example, strong natural fibrous proteins such as spider silk are known to have high β-sheet content. However, for some applications, such as film blowing, higher helical contents have been shown to be favorable.[6]

Not only is it of interest to determine what secondary structures are present, but their spatial distribution is also relevant. Dynamic mechanical analysis of blood meal based thermoplastics suggests a semicrystalline character with some phase separation after processing.[7] Microcrystalline regions in synthetic polymers can increase mechanical properties such as toughness, therefore spatial secondary structure variation in proteins may mimic this. Spatial resolution of protein secondary structures may determine if there is separation into α-helix rich and β-sheet rich regions, or plasticiser rich and protein rich phases. This will provide insight into chain rearrangements induced by processing, and may suggest future manipulations to improve properties.

FTIR is an established protein structure characterisation technique, particularly useful for exploring changes in secondary

Table I. Band Assignments in Determination of Protein Secondary Structures

Region	Secondary structure	Band assignment (cm^{-1})
Amide III[18]	α Helix	1295-1330
	β-Turns	1270-1295
	Random coils	1250-1270
	β-Sheets	1220-1250
Amide I[8]	Antiparallel β-sheet/ aggregated strands	1675-1695
	3_{10}-Helix	1660-1670
	α-Helix	1648-1660
	Unordered	1640-1648
	β-Sheet	1625-1640
	Aggregated strands	1610-1628

structure.[8] Determining absolute secondary structures (rather than just relative change) with FTIR relies on several assumptions, which may not necessarily always be valid for proteins, for example, that all structures absorb equally at the same concentration.[9] Nevertheless, quantitative estimation of secondary structures using the technique shows good agreement with X-ray data.[10,11]

Synchrotron IR sources are typically 100–1000 times brighter than conventional globar/thermal IR sources due to their highly collimated nature and small effective source size.[12,13] Very little light from a globar source will pass through a 10 μm aperture, whilst >80% of the light from a synchrotron source will, leading to much higher signal to noise ratios at high spatial resolutions.[12]

Synchrotron based FTIR microscopy (S-FTIR) has been used for spatial resolution of secondary structures in a variety of agricultural protein sources including animal feeds and feather proteins.[9,13–15] Relative estimates of the ratio of α-helices and β-sheets were able to be mapped, showing distributions across plant tissues as well as differences between feed sources known to have different digestibility. S-FTIR has also been used to examine phase separation of biopolymer blends such as gelatin with maltodextrin and quantification of peak intensities may enable analysis of compositional fractions *in situ*.[16]

Protein FTIR spectra contain several regions relating to vibrations along the polypeptide backbone. The amide I region (1600–1700 cm^{-1}), occurring mostly due to C=O bond vibration, is the most commonly used for secondary structure determination.[8] Stronger hydrogen bonds reduce electron density in the C=O bond, shifting its absorbance to lower wavenumbers. Different secondary structures have different hydrogen bonding strength leading to different characteristic absorbencies.[8] In practice, the amide I region is a convoluted peak, and techniques such as Fourier self deconvolution or second derivative analysis (2DA) are necessary to identify individual peak components.[10]

Although the amide I peak is typically the strongest absorbing peak of proteins, it also overlaps with an absorbance band of H_2O. For this reason, dry proteins or proteins dissolved in deuterated water are typically used for analysis. A further complication is that urea absorbs strongly in this region, at wavenumbers typically associated with β-sheets. As urea is used to prepare thermoplastic protein from blood meal, it may contribute to a perceived increase in β-sheets.[17] The amide III absorbance region (1200–1350 cm^{-1}) is due to in phase N—H bending and C—N stretching. Although, typically 5–10 times weaker than the amide I region, the amide III region is also sensitive to structural changes, and not subject to interference from H_2O[18] nor urea. Typical band assignments for protein secondary structures are given in Table I.

The objective of this research was to determine if there was spatial variation of protein secondary structures in blood meal and blood meal-based thermoplastics. This was explored using FTIR microspectroscopy at the Australian Synchrotron. Specifically, changes induced by processing were evaluated, which should demonstrate consolidation. The multiphase behavior implied by dynamic mechanical thermal properties could then be correlated with structural changes. Increased understanding of the interdependent relationship between structures, properties, and processing in thermoplastic protein may then suggest future directions to enhance processing methods and improve resultant material properties.

EXPERIMENTAL

Materials

Novatein thermoplastic protein (NTP) was prepared from the reagents shown in Table II. Two variants were produced,

Table II. Materials Used and NTP Compositions

Reagent	Source	Grade	Composition g/100 g blood meal (pph_{BM}) V0	V2
Blood meal	Wallace Corporation	Agricultural	100	100
Urea	Ballance Agrinutrients	Agricultural	10	10
Water	Produced on site from town supply	Distilled	60	40
Sodium dodecyl sulfate	Merck	Technical	3	3
Sodium sulphite	Merck	Technical	3	3
Triethylene glycol	Merck	For synthesis	0	20

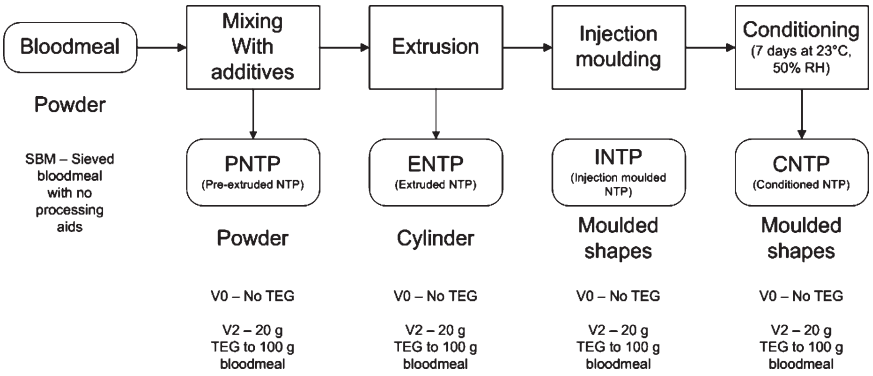

Figure 1. Samples prepared for synchrotron analysis.

differing in whether or not the plasticiser triethylene glycol (TEG) was included in the formulation.

Experimental Design

Samples were prepared at different stages of processing starting with blood meal up to a conditioned thermoplastic material, as shown in Figure 1. Two formulations were used, with and without TEG as an additional plasticiser (Table II). This resulted in eight NTP sample types, in addition to blood meal. For each sample type, a minimum of three rectangles were mapped.

Statistical Analysis. Analysis of variance (ANOVA) on secondary structure scores of the protein plastics were conducted in Statistica version 10 (StatSoft).[19] Data was filtered for a minimum area under the amide I region to exclude points mapped outside particle surfaces. A factorial experimental design was followed (Table III) and ANOVA was used to assess the effects of processing stage and the inclusion or exclusion of plasticiser on secondary structure.

Methods

Mixing with Additives. Urea, sodium sulfite, and sodium dodecyl sulphite were dissolved in distilled water at 50°C in the ratios shown in Table II, and mixed with blood meal in a high speed mixer for 10 min. If TEG was included, it was added after the first 6 min blending.

Extrusion. Extrusion was performed using a ThermoPrism TSE-16-TC twin-screw extruder with a temperature profile and screw configuration as shown in Figure 2 using a screw speed of 150 rpm. Actual melt temperatures were within 2–5°C of the set temperatures. The screw diameter was 16 mm, with an L/D ratio of 25 and it was fitted with a single 10 mm diameter circular die. A relative torque of 60–75% of the maximum allowed in the extruder was maintained (12 Nm per screw maximum) by adjusting the mass flow rate of the feed. Extruded material was granulated using a tri-blade granulator from Castin Machinery Manufacturer, New Zealand.

Table III. Array Design for ANOVA of Effects of Processing and Plasticizer Content

	Without TEG	With TEG
Pre-extrusion	PNTP-V0	PNTP-V2
Extruded	ENTP-V0	ENTP-V2
Injection molded	INTP-V0	INTP-V2
Conditioned	CNTP-V0	CNTP-V2

Injection Molding. Granulated extrudate was injection molded into Type 1 tensile test specimens[20] using a BOY-35A injection molder with 24 mm screw (L/D ratio of 24). A temperature profile of 100, 115,120, 120, and 120°C from feed zone to die, a screw speed of 200 RPM and a mold locking force of 30 kN were used. The mold was heated to 70°C using water and the injection pressure was set to 1100 bar in profile sections zero to four and 300 bar in sections 5–7.

Conditioning and Freeze Drying. Injection molded samples were placed in a chamber kept at 23°C and 50% relative humidity for 7 days. Apart from blood meal, which was already a dry powder, all samples were dried over two nights in a Freezone™ 2.5 L benchtop freeze dryer (Labconco Corporation, Kansas City) set to auto mode (collector temperature −50°C, vacuum < 11 Pa).

Synchrotron based FTIR

Data Collection. Spatially resolved FTIR experiments were undertaken on the infrared microspectroscopy beamline at the Australian Synchrotron, Victoria, Australia. Spectra were collected using a Bruker Hyperion 3000 with an MCT collector and XY stage using Opus 6.5 software (Bruker Optik GmbH 2009).Video images were captured of each sample and a minimum of three representative grids (5 μm spot size) were mapped on each. For each grid point, 32 spectra were collected with a resolution of 4 cm^{-1} between 3900 and 700 cm^{-1} and averaged. Data acquisition took $\sim$ 11 s per grid point with the subtracted background also rescanned every five points, plus additional time for sample preparation and mounting.

For solid samples, microtomed ribbons were flattened between two diamond cells removing the top of the cell for analysis. Sections 2 μm thick were cut using stainless steel blades (TBS™) on a TBS Cut 4060 RE microtome (TBS™) lit by a microlight 150 (Fibreobtic Lightguides, Australia).

For powders, fine particles were chosen and flattened between diamond cells. Initially, the top was also removed for analysis, however this proved problematic as samples decompressed during analysis. It was found that more reliable and cleaner spectra were obtained from powders with the top cell left in place.

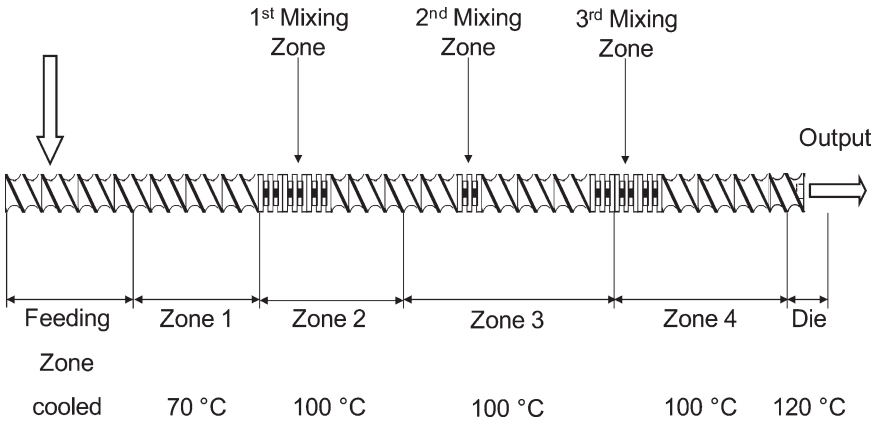

Figure 2. Extruder screw configuration and temperature profile.

Data Processing. Second derivative peaks in the amide III region have previously been used for quantitative analysis of protein secondary changes during mixing of gluten,[21] demonstrating their usefulness for analysis of changes in solid phase mixtures containing non-native protein. Derivation offers two main advantages: first, sloping baselines are removed without the need for subjective corrections.[22] This is advantageous for grid maps where the baseline shape may not be constant across the entire map. Second, spectral resolution of overlapping bands is increased.[22] This is advantageous for both the amide I and amide III regions of proteins, which contain overlapping bands corresponding to different secondary structure conformations.

There are two challenges in using 2DA for quantitative structure determination: noise increases through the introduction of peak side-lobes; and second derivative peak heights are sensitive to the half width at half height (HWHH) of original peaks, with narrower peaks giving higher second derivative peaks.[23] This has led to criticism of the reliability of determining protein secondary structure composition using 2DA.[24] However, if the same calculation procedure is used for all samples and the same peaks are of interest, relative differences can still be explored.[23] Demonstrations using poly L-lysine and hemoglobin as model proteins have shown that neither the side lobes nor HWHH issues affected quantitative results using 2DA.[24]

The second derivative of the original spectra (with no baseline correction) was determined using the Savitzky-Golay algorithm in Opus 6.5 using nine point smoothing. The second derivative was inverted by dividing by negative one and peak heights above the zero line were compared. Spatial maps were drawn using OPUS 6.5 based on the ratios A''_α/A''_β, A''_t/A''_β, and A''_r/A''_β, where A''_x is the maximum height of the inverted second derivative peak within the wavenumber range associated with α-helices, β-sheets, turns, and random coils (Table I) indicated, respectively, by the subscripts α, β, t, and r. The molar fraction for each secondary structure type was calculated using eqs. (1)–(5) and spatial maps were drawn based on these compositions using Microsoft Excel.

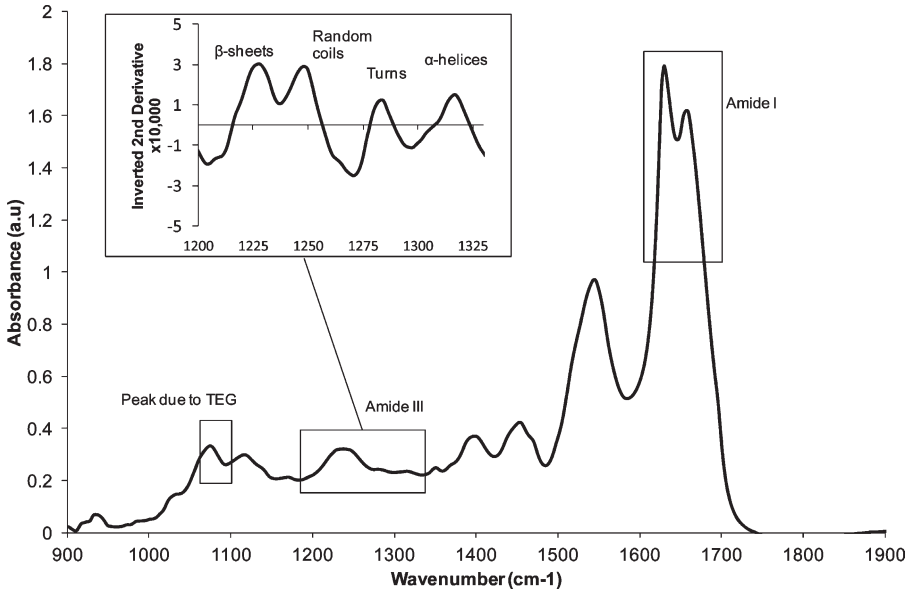

Figure 3. Example spectra of ENTP V2 from a single 5 μm spot on a mapped grid.

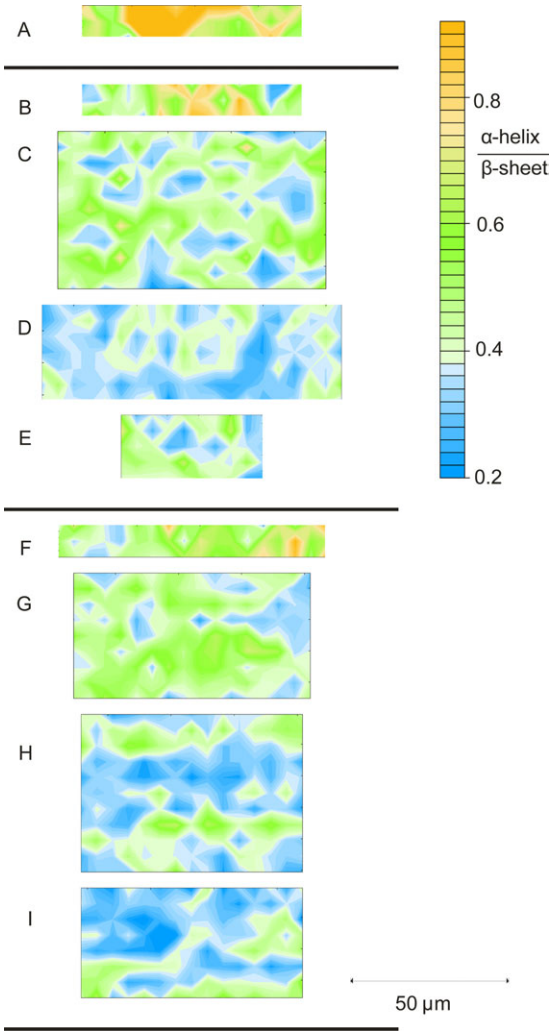

Figure 4. Representative maps showing second derivative peak height ratios (α-helices/β-sheets) for (A) Blood meal, (B) PNTP V0, (C) ENTP V0, (D) INTP V0, (E) CNTP V0, (F) PNTP V2, (G) ENTP V2, (H) INTP V2, and (I) CNTP V2. All maps have been drawn at the same scale and intensity scale. [Color figure can be viewed in the online issue, which is available at wileyonlinelibrary.com.]

$$\alpha + \beta + t + r = 1 \tag{1}$$

$$\beta = \frac{1}{A''_\alpha/A''_\beta + A''_t/A''_\beta + A''_r/A''_\beta + 1} \tag{2}$$

$$\alpha = \beta \frac{A''_\alpha}{A''_\beta} \tag{3}$$

$$t = \beta \frac{A''_t}{A''_\beta} \tag{4}$$

$$r = \beta \frac{A''_r}{A''_\beta} \tag{5}$$

The composition approximates a mole fraction of peptide linkages in each structural conformation, each of which absorbs differently in the amide III region. Spatial maps of TEG distribution were constructed by comparing the area ratio of the peak at 1040–1090 cm^{-1} to the total area of the amide III region.

WAXS

Powder wide angle X-ray scattering (WAXS) was conducted using a Phillips system running X'Pert Data Collector vs. 2.0b and XPERT-MPD vs. 2.7 control software. A PW3373/00 Cu LFF DK233995 X-ray tube was used at a voltage of 40 kV and current of 40 mA, which provided X-rays with a wavelength of 1.54 Å. Samples were scanned from $2\theta = 2°$–$60°$ at 0.020° steps. As well as analysing the sample types taken to the Synchrotron in powder form, conditioned plastics were ground and then freeze dried for WAXS.

RESULTS AND DISCUSSION

Classification of Peaks and Ratio of α-Helices to β-Sheets

A typical FTIR spectra from the protein plastic is shown in Figure 3 along with an inverted second derivative in the amide III region demonstrating the resolution of this region into four peaks. Based on assignments in literature these were taken to represent α-helices, turns, random coils, and β-sheets in order of decreasing wave number.[18,21] It should be emphasised that Figure 3 only represents one 5 μm spot on one sample of the plastic. Changes in the relative heights of these peaks could be used as a comparison reflecting relative differences in protein secondary structure spatially across a sample (Figure 4).

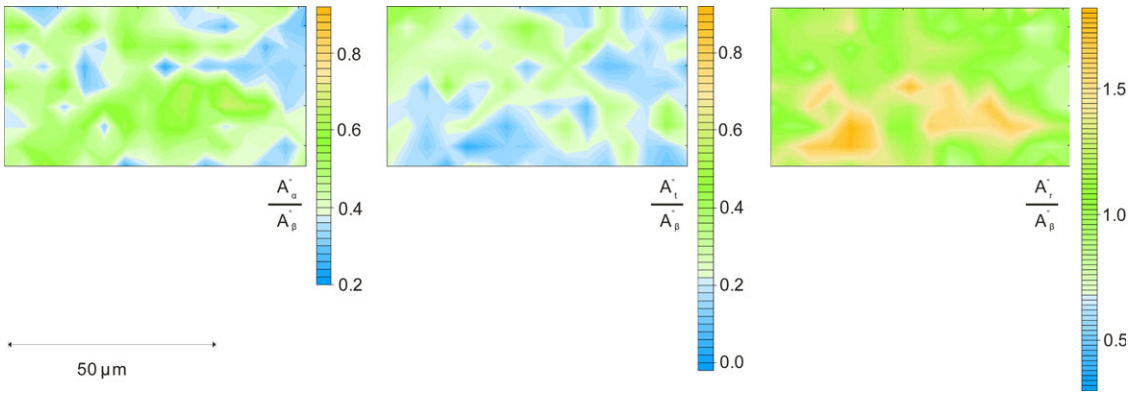

Figure 5. Maps of second derivative peak height ratios in ENTP V2. From left to right: α-helix/β-sheet, turn/ β-sheet, and random coil/β-sheet. [Color figure can be viewed in the online issue, which is available at wileyonlinelibrary.com.]

Applied Polymer SCIENCE

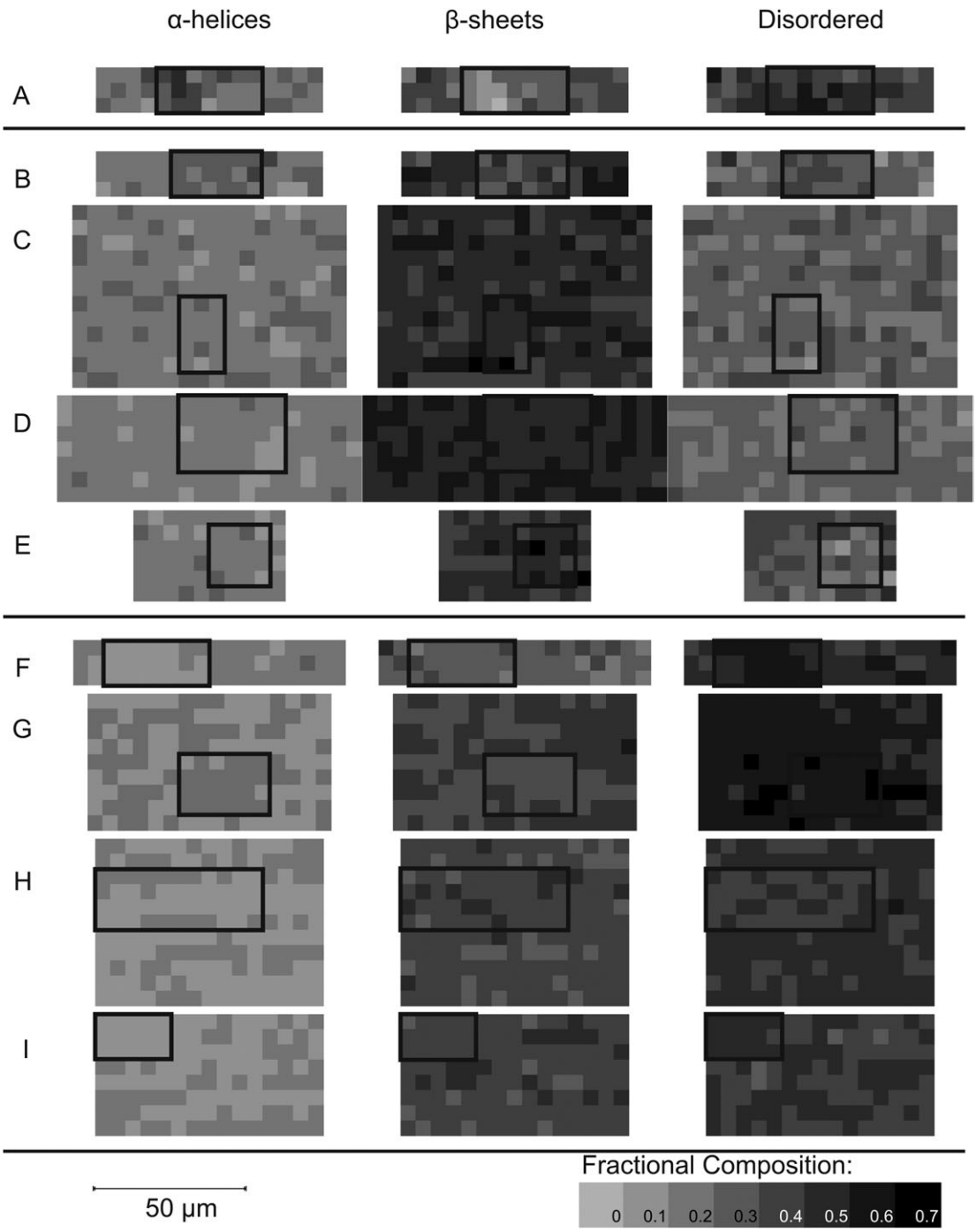

Figure 6. Representative maps showing fractional secondary structure for (A) Blood meal, (B) PNTP V0, (C) ENTP V0, (D) INTP V0, (E) CNTP V0, (F) PNTP V2, (G) ENTP V2, (H) INTP V2, and (I) CNTP V2. All maps have been drawn at the same distance and intensity scale. Each pixel represents a 5 μm spot and the shading represents the relative composition calculated from the inverted second derivative spectra.

Comparison of peak height ratios across a map, rather than actual peak height, has the advantage of correcting for any differences in thickness.[13] Such a method has been used in conjunction with S-FTIR to compare ratios of α-helices and β-sheets in a variety of agricultural protein sources including animal feeds and coproducts of biofuel production.[13–15]

The ratio of α-helix to β-sheet peak height was typically well below one, suggesting that there are more β-sheets than helices. Although the main proteins in bovine blood (haemoglobin and bovine serum albumin) are known to have helical structures, a higher proportion of β-sheets is consistent with thermal aggregation during blood meal production. In blood meal and pre-processed material, the regions with the highest helical content, relative to β-sheets, are in the centre of particles (Figure 4). It is worth noting that extrusion caused drastic changes in the appearance of the spatial maps, but the material looks similar

Table IV. ANOVA Results for Effect of Formulation and Processing on Fractional Secondary Structure

		Helix		Turn		Random coil		Sheet	
Factor	DOF	*F*	Contrib.	*F*	Contrib.	*F*	Contrib.	*F*	Contrib.
Formulation	1	730	15 %	207	6 %	4454	53 %	4175	43 %
Processing	3	244	15 %	41	3 %	184	7 %	781	24 %
Formulation × Processing	3	17	1 %	59	5 %	48	2 %	11	0.3 %
Error	3236		69 %		86 %		38 %		32.7 %
Total	3423		100 %		100 %		100 %		100 %

		Helix/sheet ratio		Turn/sheet ratio		Random coil/sheet ratio	
Factor	DOF	*F*	Contrib.	*F*	Contrib.	*F*	Contrib.
Formulation	1	56	1 %	401	10 %	2557	37 %
Processing	3	383	25 %	82	6 %	364	16 %
Formulation × Processing	3	55	4 %	71	5 %	27	1 %
Error	3236		70 %		79 %		46 %
Total	3423		100 %		100 %		100 %

after injection molding and conditioning. After processing, there is reduced overall helical content relative to β-sheets, but there was still spatial variation with regions showing a higher ratio of α -helices than other portions of the same map. Although this suggests some structural changes are caused by extrusion, thermoplastic protein is better thought of as a four component system comprised of helices, sheets, random coils, and turns. Limiting analysis to the ratio of α-helices to β-sheets does not make the distinction between whether the effect of processing is to decrease helices, increase sheets, or both. The ratio of random coils to β-sheets and of turns to β-sheets were also found to vary spatially across each map (Figure 5) showing that variations in these also need to be taken into account.

Changes in Fractional Composition

Figure 6 shows maps of fractional composition calculated from the second derivative peak height ratios for representative grids for each sample. While Figure 6 only shows a single mapped rectangle for each sample type, a minimum of three maps were scanned for each, visually inspected, and included in the statistical analysis. Both α-helices and β-sheets are ordered structures whereas random coils and turns are have been grouped together to represent the disordered amorphous fraction. When viewed in this way, it is apparent that the variation in α-helix/β-sheet ratio seen in Figure 4 was partly caused by clusters of helix rich regions, higher amounts of β-sheets near blood meal particle edges, and a more disordered particle core. Processing additives induced some chain rearrangement in blood meal prior to extrusion. This is important as protein cross-linking (physical and chemical) fixes chains in place, preventing thermoplastic flow during heating. The additives disrupted cross-linking and the chain rearrangements observed here demonstrates that disruption occurred prior to extrusion.

Results from a factorial ANOVA, considering the effect of both formulation and processing stages, are shown in Table IV and Figure 7. Formulation, processing and their interaction were significant at >99% confidence level for all four structures. Formulation had the greatest percentage contribution to the

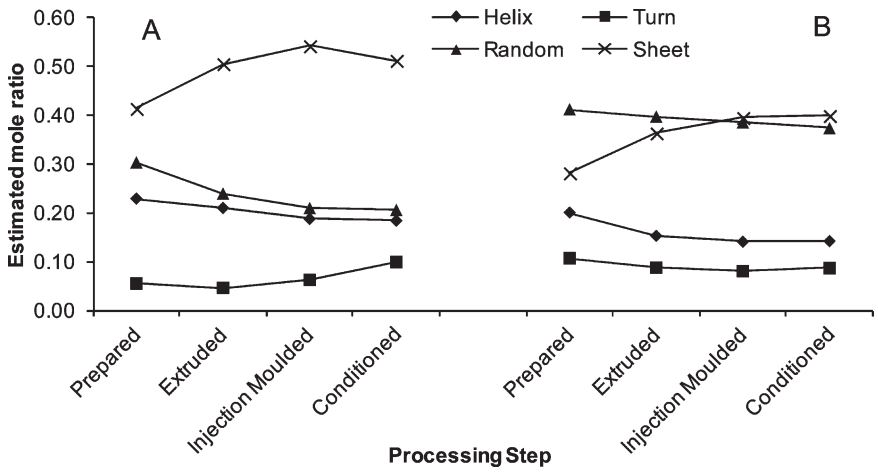

Figure 7. ANOVA means results demonstrating effect of formulation and processing on mean compositions. (A) Formulation V0 (no TEG) and (B) formulation V2 (with 20 pph_{BM} TEG).

Table V. Summary Statistics

	Fractional Composition of Each Structure					T-Test Results		
	Mean	Std. dev	Lower quartile	Median	Upper quartile	Rectangle mean	Subset mean	*P*-value
α-Helices								
SBM	0.24	0.06	0.19	0.23	0.28	0.26	0.30	0.15
PNTP V2	0.20	0.07	0.15	0.19	0.24	0.17	0.14	0.00
ENTP V2	0.15	0.03	0.14	0.15	0.17	0.15	0.17	0.00
INTP V2	0.14	0.03	0.12	0.14	0.16	0.14	0.14	0.74
CNTP V2	0.14	0.03	0.12	0.14	0.16	0.14	0.11	0.00
PNTP V0	0.23	0.04	0.20	0.23	0.26	0.24	0.28	0.03
ENTP V0	0.21	0.04	0.18	0.21	0.24	0.21	0.21	0.99
INTP V0	0.19	0.03	0.16	0.19	0.21	0.19	0.19	0.57
CNTP V0	0.18	0.04	0.15	0.18	0.21	0.19	0.20	0.34
β-Sheets								
SBM	0.35	0.09	0.29	0.36	0.41	0.30	0.23	0.01
PNTP V2	0.28	0.07	0.23	0.29	0.33	0.31	0.31	0.63
ENTP V2	0.36	0.04	0.33	0.36	0.39	0.35	0.32	0.00
INTP V2	0.39	0.05	0.36	0.39	0.43	0.39	0.42	0.00
CNTP V2	0.40	0.05	0.37	0.40	0.43	0.41	0.39	0.30
PNTP V0	0.41	0.06	0.37	0.41	0.45	0.46	0.39	0.00
ENTP V0	0.50	0.05	0.47	0.51	0.54	0.48	0.51	0.02
INTP V0	0.54	0.04	0.51	0.54	0.57	0.54	0.52	0.01
CNTP V0	0.51	0.07	0.46	0.51	0.56	0.48	0.52	0.04
Disordered structures								
SBM	0.41	0.09	0.35	0.40	0.47	0.43	0.47	0.09
PNTP V2	0.52	0.08	0.47	0.52	0.57	0.52	0.56	0.01
ENTP V2	0.48	0.04	0.46	0.48	0.51	0.49	0.51	0.19
INTP V2	0.46	0.04	0.44	0.46	0.49	0.46	0.44	0.00
CNTP V2	0.46	0.04	0.43	0.46	0.49	0.45	0.49	0.00
PNTP V0	0.36	0.07	0.32	0.36	0.40	0.30	0.34	0.11
ENTP V0	0.29	0.06	0.25	0.29	0.32	0.30	0.28	0.04
INTP V0	0.27	0.05	0.24	0.27	0.30	0.27	0.30	0.01
CNTP V0	0.30	0.07	0.25	0.31	0.36	0.33	0.28	0.02

amount of random coils and β-sheets, but processing also had a reasonable contribution to β-sheets. By comparing the means shown in Figure 7, going from prepared to an extruded material had a greater effect than subsequent injection molding and conditioning. Without TEG, addition of processing additives led to an increase in β-sheets, whereas including TEG with the additives increased disordered structures. After thermal processing, the samples with TEG continue to have more disordered structures and less β-sheets than samples without TEG. This effect was not apparent when simply looking at the α-helix/β-sheet ratio in Figure 4. Similarly, the ANOVA showed only a 1% contribution to the α-helix/β-sheet ratio, but larger contributions to both the individual helix and sheet content were observed.

The error terms for each structure showed that there was some variability not accounted for by the tested factors. In other words, although the means were significantly different between groups, there was still considerable variability within groups. This variability within groups was quantified in terms of standard deviation and quartiles within each sample type (Table V). In some cases, the difference between the upper and lower quartile within a sample was greater than the difference between the means between sample types. When considering this in conjunction with what is observed in Figure 6, it can be concluded that there was variation in secondary structure at different points within plastic sample as extreme as the difference in average composition before and after extrusion. A T-test between the highlighted subsections of each rectangle shown in Figure 6 and the rectangles themselves showed that regions of adjacent points could be identified with a significantly different composition to the map's average. The *P*-values obtained are shown in Table V. For each sample type, a region could be identified with a significantly different ($P < 0.05$) fractional content of at least two structure types (alpha helices, β- sheets, or disordered structures).

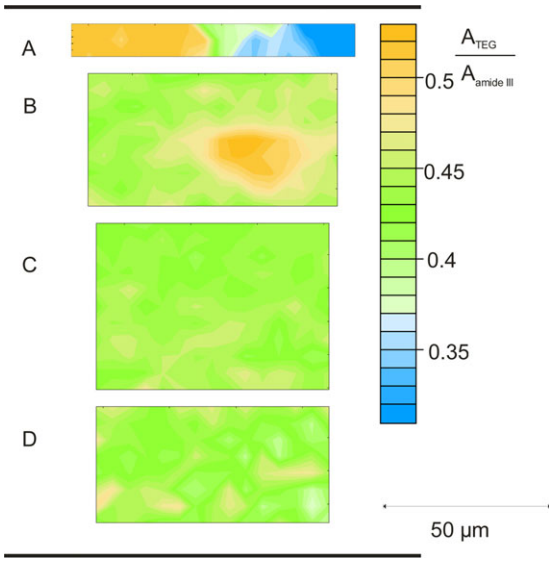

Figure 8. Spatial distribution of TEG in NTP. Representative maps of (A) PNTP, (B) ENTP, (C) INTP, and (D) CNTP. All four maps are on the same distance and intensity scale. [Color figure can be viewed in the online issue, which is available at wileyonlinelibrary.com.]

TEG Distribution

Spectra for samples with TEG showed a peak between 1040 and 1090 cm^{-1}, which was not present in samples without TEG. This peak was thought to be due to the C-OH functional groups in TEG. The ratio of this peak area to the amide III peak (baselines drawn across the bottom of each peak) was taken as representative of variations in TEG concentration across the sample. Variation in this ratio was seen in the samples, suggesting the presence of TEG rich regions and TEG poor regions (Figure 8). In PNTP, the centre of a large particle was relatively TEG poor compared with the perimeter suggesting TEG was unable to diffuse into the centre. After extrusion, regions of high TEG concentration suggested some heterogeneity. Injection molding appeared to have led to a finer dispersion, with heterogeneity returning after conditioning.

WAXS

WAXS for blood meal showed a sharp peak at $s = 1.3$ $Å^{-1}$, corresponding to a d-spacing of 4.8 Å, and another peak at about $s = 0.6$ $Å^{-1}$, corresponding to a d-spacing of 10.5 Å (Figure 9). Peaks corresponding to these distances are commonly seen in WAXS patterns of proteins and have alternately been described as corresponding to β-sheet structures or α-helix structures.[25] Both of these were reduced dramatically in pre-processed material with TEG, but less so when TEG was absent. Protein secondary structures are stabilized by hydrogen bonding interactions along the main chain (α-helices) or between adjacent chains (β-sheets). TEG contains function groups capable of hydrogen bonding, so it is reasonable to expect some disruption to secondary structure as protein-plasticiser interactions replace protein-protein interactions. A d-spacing of 4–5 Å corresponds to regular distances within structures, while a d-spacing of about 10.5 Å corresponds to interstructure packing (either stacked β-sheets or adjacent helices). That both peaks decrease in size with TEG supports observations from FTIR that TEG reduced overall α-helix and β-sheet content, and disrupted tight packing. Comparison of preprocessed material with ground conditioned material showed little difference within each formulation, and the difference between the two formulations was pronounced at both processing steps.

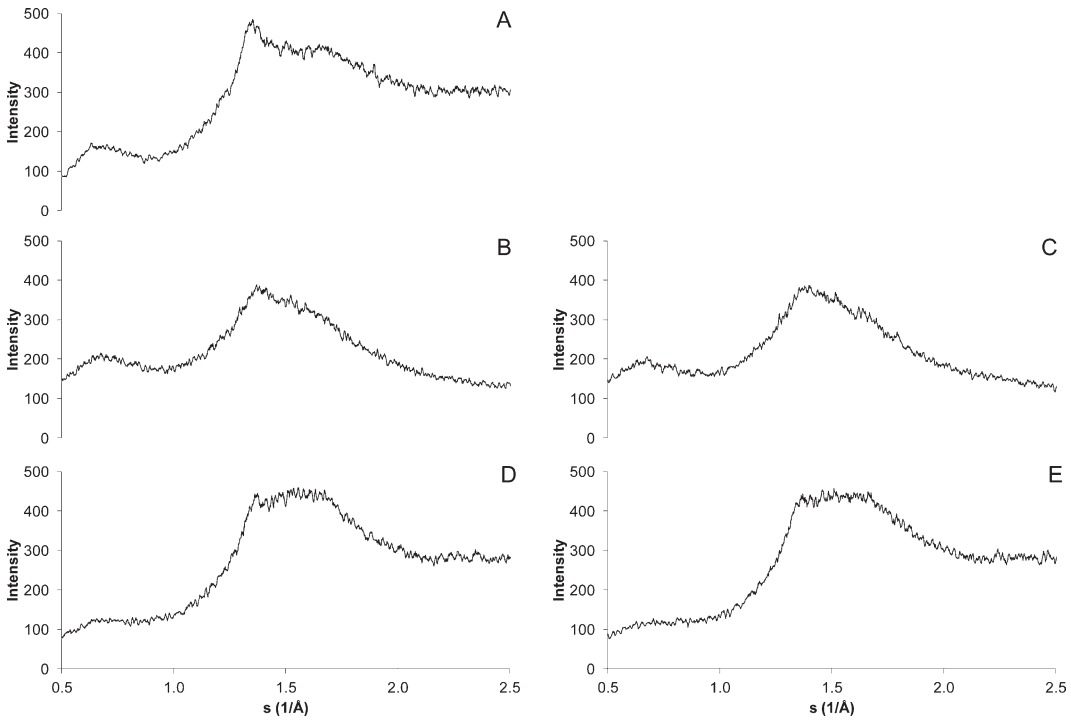

Figure 9. WAXS plots for (A) blood meal, (B) PNTP V0, (C) CNTP V0, (D) PNTP V2, and (E) CNTP V2.

Applied Polymer SCIENCE

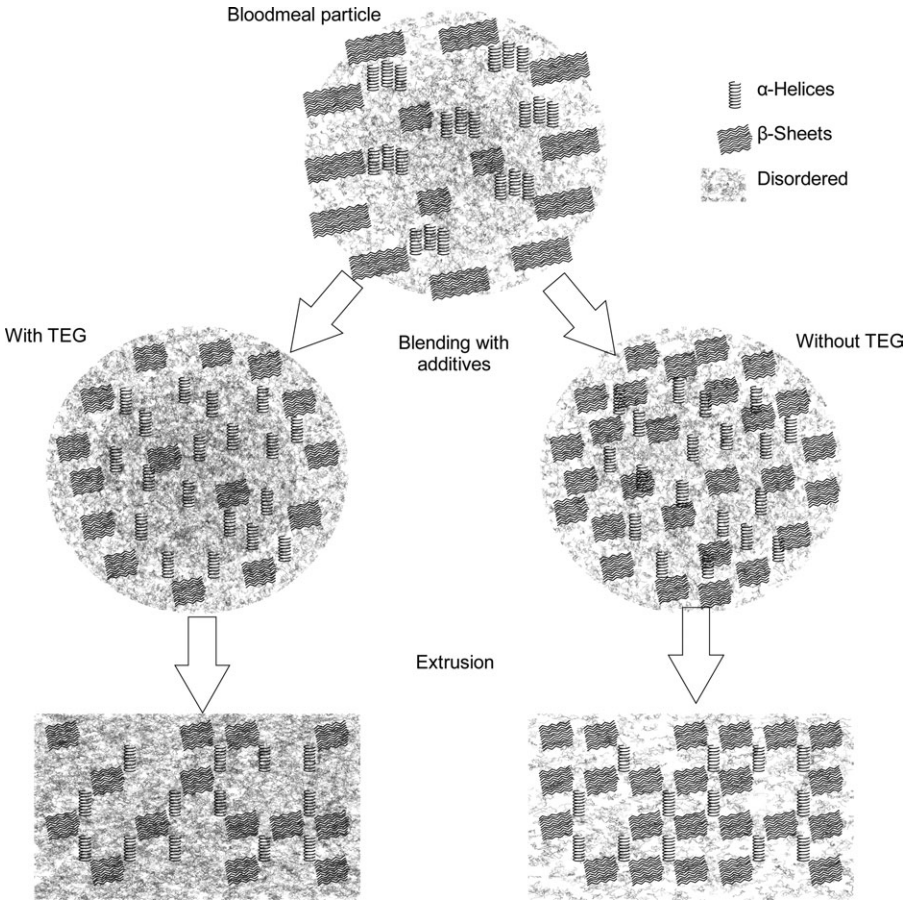

Figure 10. Schematic of proposed model for changes in structural dispersion as blood meal is processed into a thermoplastic.

Proposed Model for Structural Changes

Blood meal predominantly contains a uniform dispersion of helical structures and turns. Some blood meal particles suggested there were more α-helices in the centre, but this was not consistent throughout all particles tested. A higher concentration of β-sheets was consistently observed toward the edge of particles and a higher proportion of random coils in the middle of particles. Two aspects of blood meal production may contribute to this. Blood meal production involves coagulation followed by steam drying. The coagulation step may force hydrophobic side chains to aggregate, with hydrophilic regions still facing outward. These hydrophobic side group interactions then result in a random coil structure, rather than forming α-helices and β-sheets by hydrogen bonding. Additionally, cysteine–cysteine crosslinking is known to occur at elevated temperatures and may further stabilize the coagulated conformation. As additional heat is supplied and water is evaporated, β-sheet aggregation may then occur as water is removed from the hydrophilic regions at the edges of the coagulated particle. A second, alternative explanation is that β-sheets, being more crystalline, may be more brittle than random coils, and breakages may occur at these brittle regions when blood meal passes through a hammer mill at the end of blood meal production.

Transformation of blood meal into a thermoplastic involves the addition of urea to disrupt hydrogen bonding, sodium dodecyl sulfate to disrupt hydrophobic interactions and sodium sulfite to disrupt cysteine–cysteine crosslinkages. This destabilizes the side chain interactions in the disordered core, allowing formation of additional β-sheets prior to extrusion in the formulation without TEG. With TEG, an increase in disorder and a decrease in α-helices were observed. This observation can be explained by the presence of TEG contributing additional free volume and preventing new tightly packed interactions from occurring necessary for forming additional β-sheets. This is further supported by WAXS, which revealed that the tight packing of secondary structures observed in blood meal was preserved without TEG, but was reduced with it. A schematic of the changes thought to be occurring is shown in Figure 10.

The next transformation involves applying heat and shear in an extruder. This causes radical chain rearrangements necessary for consolidation of individual particles into a continuous extrudate. On an average structure level, this leads to an increase in β-sheets and reductions in both random coils and α-helices. More β-sheets were seen without TEG than with it, although both formulations showed evidence of spatial variations in their distribution. A decrease in turns suggested intermolecular β-sheets were formed rather than β-sheets consisting of chains folding back on themselves. Together, this suggests chain unravelling during heating and reformation of β-sheets

upon cooling, with some nucleation effects potentially leading to variations in β-sheet concentration across maps.

Injection molding involves heating to rearrange chains and allow them to flow under pressure. However the transformation from extruded to injection molded material was not nearly as drastic as what occurs when first extruded. Average composition did change slightly in favor of β-sheets, but the spatial map of β-sheet concentration looked comparable between extruded and injection molded samples. The slight effect of this second heating and cooling cycle confirmed the thermoplastic nature of NTP.

Conditioning was the final processing step in producing NTP test pieces and was included because NTP is hydrophilic and moisture sensitive. Changes in macroscopic properties such as tensile strength and glass transition temperature have previously been observed after conditioning.[7,26] Average secondary structure and the spatial distribution thereof appeared to change little between unconditioned and conditioned injection molded samples suggesting the changes in macroscopic properties were mostly due to changes in moisture content, rather than reformation of α-helices and β-sheets.

CONCLUSIONS

Blood meal-based thermoplastics should be considered as a semicrystalline polymer consisting of clusters of crystalline regions of α-helices and β-sheets distributed throughout a randomly coiled protein structure. The additives used to process blood meal into a thermoplastic caused structural rearrangement implying cysteine–cysteine crosslinking between protein chains was disrupted and chain mobility has increased. Extrusion caused drastic structural rearrangement, resulting in a more uniform structure implying consolidation had occurred. In blood meal particles, β-sheets were concentrated around the perimeter of particles, while in extruded and injection molded materials, β-sheet rich regions were distributed evenly throughout a more disordered matrix. Including TEG as a plasticizer reduced α-helices and β-sheets and increased the amount of disordered protein chains at each processing stage. These findings are consistent with earlier work, which indicated that NTP exhibited multiphase behavior beyond simple plasticizer separation. The results also suggest that if these structures and the distribution thereof can be manipulated, material properties could potentially be tailored for different applications.

ACKNOWLEDGMENTS

This research was undertaken on the infrared microspectroscopy beamline at the Australian Synchrotron, Victoria, Australia. Proposal number AS113/IRMFI/4267. The authors would especially like to acknowledge the technical assistance of Dr. Mark Tobin. Travel funding support was received from the New Zealand Synchrotron Group Ltd.

REFERENCES

1. Verbeek, C. J. R.; van den Berg, L. E. *Macromol. Mater. Eng.* **2010**, *295*, 10.
2. Verbeek, C. J. R.; Viljoen, C.; Pickering, K. L.; van den Berg, L. E. Plastic Matetial. NZ Patent NZ551531, **2007**.
3. Verbeek, C. J. R.; van den Berg, L. E. *J. Polym. Environ.* **2010**, *19*, 1.
4. Pickering, K.; Verbeek, C.; Viljoen, C. *J. Polym. Environ.* **2012**, *20*, 335.
5. Verbeek, C. J. R.; van den Berg, L. E. *Recent Pat. Mater. Sci.* **2009**, *2*, 171.
6. Oliviero, M.; Maio, E. D.; Iannace, S. *J. Appl. Polym. Sci.* **2010**, *115*, 277.
7. Bier, J. M.; Verbeek, C. J. R.; Lay, M. C. *J. Therm. Anal. Calorim.* **2012**, 1. Available at: http://dx.doi.org/10.1007/s10973-012-2680-0.
8. Jackson, M.; Mantsch, H. H. *Crit. Rev. Biochem. Mol. Biol.* **1995**, *30*, 95.
9. Yu, P. Q. *Spectr.-Int. J.* **2006**, *20*, 229.
10. Mantsch, H. H.; Casal, H. L.; Jones, R. N. In Spectroscopy of Biological Systems; Clark, R. J. H., Hester, R. E., Eds.; Wiley: Chichester, **1986**; pp 547.
11. Kong, J.; Yu, S. *Acta Biochim. Biophys. Sin.* **2007**, *39*, 549.
12. Miller, L. M. In Infrared and Raman Spectroscopic Imaging; Salzer, R., Siesler, H. W., Eds.; Wiley-VCH: Weinheim, **2009**, pp 510.
13. Yu, P. Q.; McKinnon, J. J.; Christensen, C. R.; Christensen, D. A. *J. Agric. Food Chem.* **2004**, *52*, 7353.
14. Yu, P.; Christensen, D. A.; Christensen, C. R.; Drew, M. D.; Rossnagel, B. G.; McKinnon, J. J. *Can. J. Anim. Sci.* **2004**, *84*, 523.
15. Yu, P. Q.; Niu, Z. Y.; Damiran, D. *J. Agric. Food Chem.* **2010**, *58*, 3460.
16. De Giacomo, O.; Cesaro, A.; Quaroni, L. *Food Biophys.* **2008**, *3*, 77.
17. Verbeek, C. J. R.; van den Berg, L. E. *J. Appl. Polym. Sci.* **2012**, *125*, E347.
18. Cai, S. W.; Singh, B. R. *Biophys. Chem.* **1999**, *80*, 7.
19. Statistica version 10, Statsoft Inc. Statsoft.com. **2011**.
20. ASTM International. ASTM International: West Conshohocken, PA, **2004**.
21. Seabourn, B. W.; Chung, O. K.; Seib, P. A.; Mathewson, P. R. *J. Agric. Food Chem.* **2008**, *56*, 4236.
22. Diem, M.; Matthäus, C.; Chernenko, T.; Romeo, M. J.; Milijkovic, M.; Bird, B.; Schubert, J.; Papamarkakis, K.; Laver, N. In Infrared and Raman spectroscopic imaging; Salzer, R., Siesler, H. W., Eds.; Wiley-VCH: Weinheim, **2009**; pp 510.
23. Saarakkala, S.; Rieppo, L.; Rieppo, J.; Jurvelin, J. S. In Microscopy: Science, Technology, Applications and Education; Méndez-Vilas, A., Díaz, J., Eds.; Formatex Research Center: Badajoz, Spain, **2010**; pp 403.
24. Zhang, J.; Yan, Y.-B. *Anal. Biochem.* **2005**, *340*, 89.
25. Elshemey, W. M.; Elfiky, A. A.; Gawad, W. A. *Protein J.* **2010**, *29*, 545.
26. Verbeek, C. J. R.; van den Berg, L. E. *Macromol. Mater. Eng.* **2011**, *296*, 524.